Available online at www.sciencedirect.com
ScienceDirect
Trans. Nonferrous Met. Soc. China 29(2019) 919−930
Transactions of Nonferrous Metals Society of China
www.tnmsc.cn

# Microstructure evolution of modified die-cast AlSi10MnMg alloy during solution treatment and its effect on mechanical properties

Zi-hao YUAN[1], Zhi-peng GUO[1], Shou-mei XIONG[1,2]

1. School of Materials Science and Engineering, Tsinghua University, Beijing 100084, China;
2. State Key Laboratory of Automobile Safety and Energy, Tsinghua University, Beijing 100084, China

Received 7 May 2018; accepted 7 January 2019

**Abstract:** To optimize the solution treatment process of a modified high-pressure die-cast AlSi10MnMg alloy, the influence of the solution treatment on the microstructure, mechanical properties and fracture mechanisms was studied using OM, SEM, EBSD and tensile test. The experimental results suggest that the solution treatment could be completed in a shorter time at a temperature much lower than the conventional practice. Surface blistering could be avoided and substantial strengthening effect could be achieved in the following aging process. Prolonging solution treatment time and elevating solution temperature would be meaningless or even harmful. The rapid evolution of eutectic silicon during solution treatment, especially at the early stage, affected the way of interaction among $\alpha$-Al grains during plastic deformation, and changed the ultimate mechanical properties and fracture mode.

**Key words:** AlSi10MnMg alloy; die casting; solution treatment; microstructure evolution; mechanical properties; process optimization

## 1 Introduction

High-pressure die casting (HPDC) is one of the most efficient casting processes for mass production of shaped components. Due to extremely high interfacial heat transfer coefficient [1], the melt solidifies at a high cooling rate, leading to a very refined microstructure and better mechanical properties. However, the complicated flow pattern [2] for thin-walled castings would lead to air entrapment or gas pores, which significantly decreases the ultimate mechanical properties of the component. Besides, the sub-surface gas pores would cause surface blisters during conventional solution treatment (4−10 h at 540 °C for Al−Si−Mg alloys [3−5]), which follows the principle of high temperature and long time to homogenize the alloy elements.

Both vacuum-assisted and pore-free die casting could reduce the gas porosity significantly [6,7]. Recent studies [8−11] have also demonstrated that a low temperature solution treatment could reduce surface blisters, and the subsequent artificial aging could improve the tensile strength significantly. Mostly processed by HPDC, the modified AlSi10MnMg alloy has been widely used in automobile industry due to its excellent castability and mechanical performance. Mg could promote the formation of strengthening phases, e.g., $Mg_2Si$ at the inter-granular boundary of the as-cast microstructure. In order to further improve the mechanical properties, the $Mg_2Si$ phase must dissolve into the $\alpha$-Al matrix and precipitate as nano-size meta-stable phases inside the grains [12−15].

Extensive studies have been performed to investigate the effect of solution treatment on the microstructure and mechanical properties of the cast Al−Si−Mg alloys. The best solution treatment process parameters varied within a wide range, which strongly depend on the alloy composition [16,17], morphology of eutectic silicon [17−19] and manufacture process [4,5]. And the solution treatment affected the final mechanical performance through dissolving and homogenizing alloy elements [16,19,20], as well as changing silicon phase [19,21].

Due to the advantages and disadvantages of the die-cast alloys, the optimized solution treatment parameters should be revised, following different principles from

**Foundation item:** Project (U1537202) supported by the National Natural Science Foundation of China; Project (BA2015041) supported by the Special Funding Program on Transformation of Scientific and Technological Achievements in Jiangsu Province, China
**Corresponding author:** Shou-mei XIONG; Tel: 86-10-62773793; Fax: 86-10-62770190; E-mail: smxiong@tsinghua.edu.cn
DOI: 10.1016/S1003-6326(19)65001-6

that of conventional heat treatment. Very refined microstructure makes it possible to shorten the solution treatment process at a relatively low temperature, which also reduces the risk of blisters. For the heat treatment of a modified AlSi10MnMg high-pressure die-cast alloys, detailed studies need to be performed to optimize the process parameters. In this work, quantitative analysis was performed on the microstructure evolution and mechanical properties during the solution treatment. In-situ tensile deformation together with fractography analysis was performed to reveal the fracture mode and crack expansion. The process−microstructure−property relationship was investigated, together with the discussion on the optimization of process parameters.

## 2 Experimental

The composition of the modified AlSi10MnMg alloy used in this study is listed in Table 1. Si would improve the flowability of the alloy and reduce the risk of hot cracking. The content of Mg is 0.301 wt.% to ensure a distinct strengthening effect, and all the $\beta$-$Mg_2Si$ phases could dissolve into the $\alpha$-Al matrix at a relatively low solution temperature. Sr could modify the morphology of the eutectic silicon. The content of Fe was as low as 0.109 wt.% to reduce the brittle needle-like iron-rich $\beta$-$Al_5FeSi$ during solidification, but at the risk of die soldering. As a compensation, Mn was added into the alloy to reduce die soldering.

The HPDC components were produced by using a TOYO BD−350V5 cold chamber die casting machine with key processing parameters listed in Table 2. Oil was circulated inside the dies to stabilize the temperature (at ~120 °C). Figure 1 shows the configuration of the die casting, which comprised 3 bars and 1 plate of 170 mm × 30 mm × 2.5 mm. Detailed configuration of the cylindrical tensile specimen is shown in Fig. 1(b).

**Table 1** Composition of modified AlSi10MnMg alloy (wt.%)

| Si | Mg | Mn | Fe | Cu | Sr | Ti | Zn | Al |
|---|---|---|---|---|---|---|---|---|
| 10.14 | 0.301 | 0.639 | 0.109 | 0.016 | 0.025 | 0.073 | 0.007 | Bal. |

**Table 2** Key processing parameters of die casting

| Parameter | Value |
|---|---|
| Melt temperature/°C | 700 |
| Slow shot speed/(m·s$^{-1}$) | 0.15 |
| Gate speed/(m·s$^{-1}$) | 57.9 |
| Intensification pressure/MPa | 79 |
| Vacuum degree/kPa | ~90 |

The tensile testing bars were put into an electric-resistance muffle furnace at 490 °C for 5, 15, 30, 60, 120, 300, 720 and 1440 min for heat treatment followed by an immediate water quenching. As a comparison, some bars were solutionized at 520 and 540 °C for 30 min, respectively. Artificial aging process was performed at 200 °C for 2 h immediately after quenching to achieve the maximum strength (T6 state).

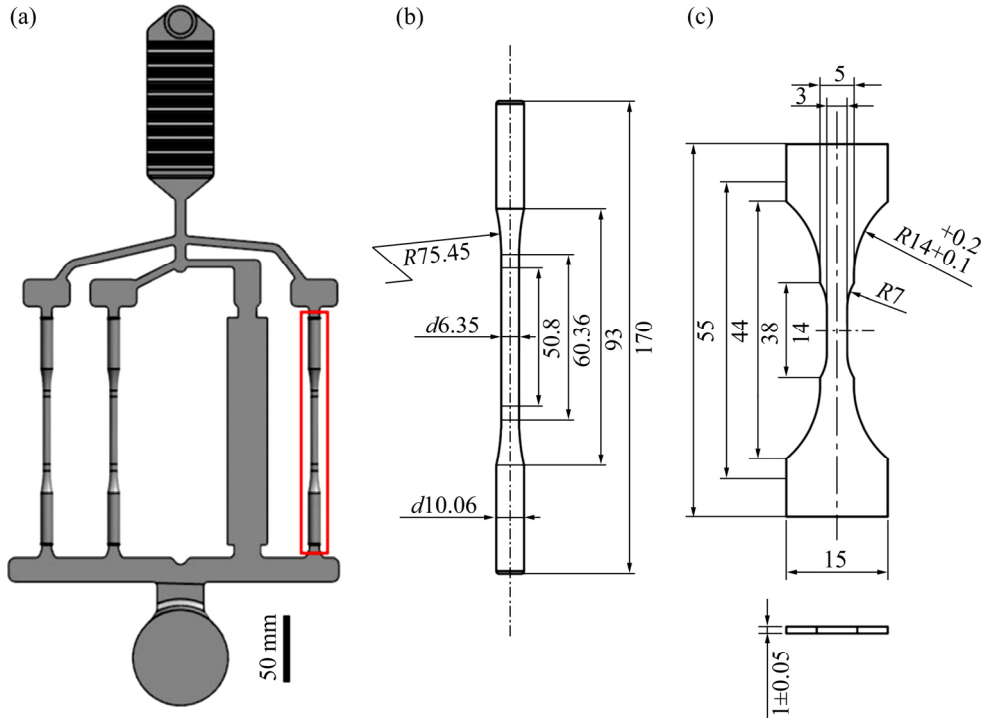


**Fig. 1** Configuration of die casting with 3 bars and 1 plate (a), dimensions of tensile testing bar (b) and tensile plate (c) for in-situ observation (unit: mm)

Several sections of samples were polished and observed using OM (optical microscope). And the OM images were used to calculate the porosity of each sample with ImageProPlus software. To investigate the microstructure evolution, the die-cast and the water-quenched samples were ground, polished, etched with Keller's etchant and observed using a JEOL 7001F SEM. The specimens for EBSD were prepared with the method of ion milling.

Mechanical properties of the as-cast state, as-quenched state and/or T6 state alloys were investigated. The yield strength (YS), ultimate tensile strength (UTS) and elongation to fracture were measured at room temperature with a strain rate of 0.0005 $s^{-1}$. A 50-mm extensometer was used to measure the elongation within the gauge length. To study the fracture mode transfer due to solution treatment, the fracture surfaces of the tensile specimens were investigated using a JEOL 7001F SEM after ultrasonic cleaning in acetone.

In order to study the plastic deformation, in-situ tensile samples were prepared from the 2.5-mm thick plate (see Fig. 1(a)) using electrical discharge machining. A 0.3-mm notch was made on the sample to imitate the fatal defect inside the components during service, and facilitate the nucleation of crack. The die-cast and T6-state in-situ samples were ground, polished and etched. In-situ tensile deformation was performed in a SEM chamber with a grip moving speed of 0.1 μm/s.

## 3 Results

### 3.1 Microstructure evolution during solution treatment

Figure 2 shows the sections and appearances of tensile bars before and after solution treatment. The porosity was originally about 0.41% in the as-cast tensile bar (see Fig. 2(a)), which slightly went up to 0.52% after 300 min solution treatment (see Fig. 2(b)), and 0.56% after 720-min solution treatment (see Fig. 2(c)). The increase in porosity was generally attributed to the expansion of gas pores [8,9]. Tensile bars were bent because of the gravitational creep after 720-min solution treatment (see Fig. 2(d)). Due to good vacuum degree and relatively low solution temperature, no obvious surface blisters were found until 1440-min solution treatment (see Fig. 2(e)). The solution temperature of 540 °C, which was ordinarily used in conventional practice, caused blisters after only 30 min (see Fig. 2(f)).

Figure 3 shows a typical microstructure of a modified high-pressure die-cast AlSi10MnMg alloy and a magnified view of modified eutectic Si. Because of the high cooling rate during solidification, most eutectic phases exhibited a divorced morphology. The externally solidified crystals (ESCs), which originally nucleated inside the shot sleeve, could be observed on the section of casting (see Fig. 3(a)). The $\alpha$-Al grains, with a size of

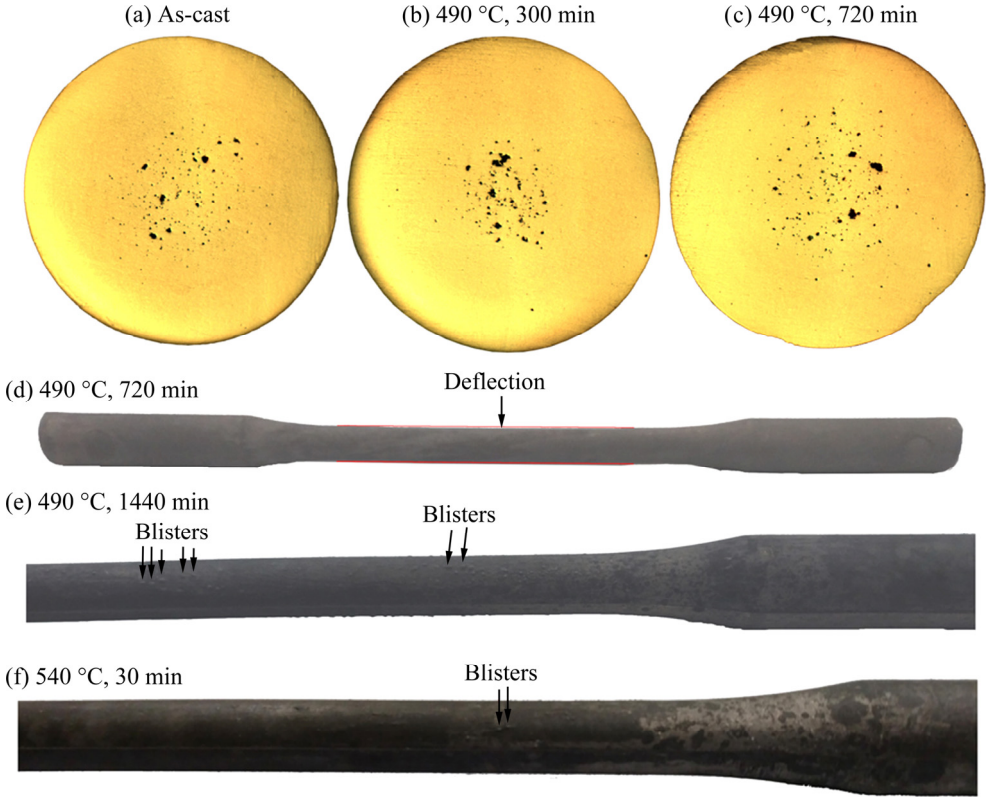


**Fig. 2** Sections (a−c) and appearance (d−f) of tensile bars

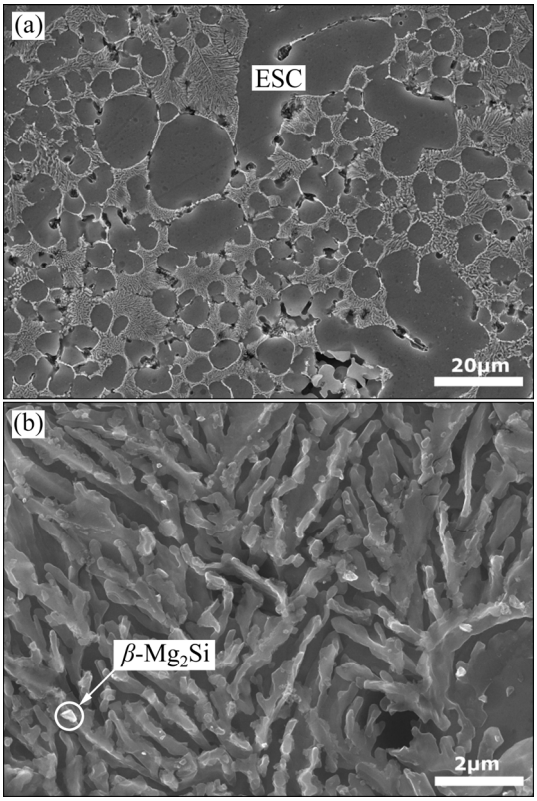


**Fig. 3** Typical microstructure of as-cast modified AlSi10MnMg alloy (a) and magnified view of modified eutectic Si (b)

15−40 μm, exhibited a globular or dendritic morphology. The fibrous eutectic silicon exhibited a coarse surface (see Fig. 3(b)), which was mostly caused by the modification of Sr. The diameter of the eutectic Si was only 100−300 nm, while its length could be several microns. The Si fibers were deeply embedded into the $\alpha$-Al matrix, and distributed at the boundaries of large $\alpha$-Al grains. The $\beta$-$Mg_2Si$ phase was also found in the eutectic region, as marked by the circle in Fig. 3(b).

The influence of the solution treatment time on the microstructure of the alloy and its average diameter as function of solution treatment time at 490 °C was shown in Fig. 4. A small part of $\beta$-$Mg_2Si$ phases were still not completely dissolved into the matrix after solution treatment at 490 °C for 5 min and fibrous Si changed into particles or short rods (see Fig. 4(a)). The dendrite arms of large $\alpha$-Al grains coalesced, with Si particles packed in. Some particles forming clusters distributed in $\alpha$-Al grains. Those particles would detach from the $\alpha$-Al matrix when deeply etched, generating holes on the polished surface of the samples (see Figs. 4(a−e)). All the $\beta$-$Mg_2Si$ phases disappeared after solution treatment for 15 min (see Fig. 4(b)). Thus, the solution temperature of 490 °C was sufficient to dissolve all the $\beta$-$Mg_2Si$ phases in this alloy due to the low content of Mg.

As coarsening occurred, the interface between the $\alpha$-Al matrix and the silicon particles became smooth. During the solution treatment, the average diameter of silicon particles increased rapidly within the first 30 min, i.e., from 0.2 to 1.68 μm, after which it increased rather slowly, i.e., the average diameter increased to only ~2.8 μm after 1 d (1440 min) of solution treatment (see Fig. 4(e)).

The grain boundaries could be recognized in the EBSD image quality maps (see Figs. 5(a−e)), according to which the average grain sizes of $\alpha$-Al matrix could be calculated (see Fig. 5(f)). Over 500 grains at the center of the bar were taken for the statistical analysis in each sample. The statistical average grain area increased rapidly in the first 60 min of solution treatment. That was the result of the disintegration of eutectic silicon. Meanwhile, some dendrite grains still existed (see Fig. 5(b)). After that, the grain size grew slowly. Nearly all grains exhibited a granular morphology, which indicated the coalescence of dendrite arms that eliminated the inner boundaries.

### 3.2 Mechanical properties

The samples were deflected and/or blistered after 720-min solution treatment, which would fail in obtaining the uniform uniaxial tensile stress during tensile test. Thus, the corresponding tensile tests were not performed. Figure 6 shows the mean values of YS, UTS and elongation as a function of solution treatment time. The dash line in each figure indicated the mechanical properties of the die-cast state. The first point of each curve corresponded to the solution time of 5 min. The dash line in each figure, i.e., 161 MPa for YS, 314 MPa for UTS, and ~7.5% for elongation, represented the values of the die-cast state.

A 5-min solution treatment could reduce both YS and UTS and increase the elongation significantly. However, longer solution treatment produced negligible effect on the as-quenched yield strength which just fluctuated between 98 and 107 MPa (see Fig. 6(a)). The UTS of as-quenched samples increased from 228 MPa at 5 min, to the maximum of 245 MPa at 30 min, then decreased slowly to 232 MPa at 300 min (see Fig. 6(b)). The elongation of as-quenched samples increased from 13% at 5 min, to the maximum of 21% at 30 min, and then decreased slowly to 16% at 300 min (see Fig. 6(c)).

A T6-treatment improved both YS and UTS significantly, but reduced elongation. The YS increased significantly from 192 to 257 MPa at treatment time from 5 to 15 min, after which the YS maintained rather stable with a slight decrease to 245 MPa at 300 min. The UTS of the T6 samples increased from 275 MPa at 5 min

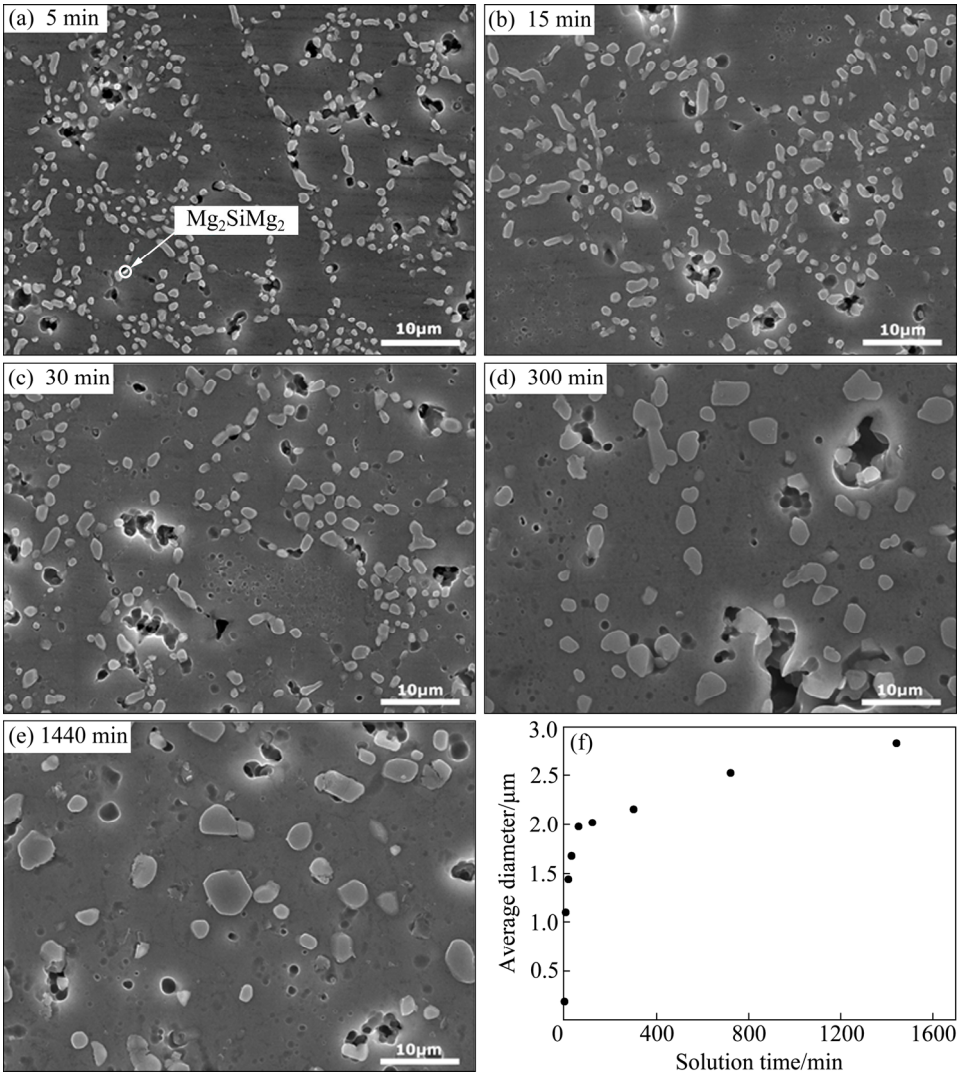


**Fig. 4** Microstructures of modified die-cast AlSi10MnMg alloy after solution treatment at 490 °C for different time (a−e) and average diameter as function of solution treatment time at 490 °C (f)

to the maximum of 326 MPa at 15 min, and then decreased slowly to 302 MPa at 300 min (see Fig. 6(b)). The elongation increased from 10% at 5 min to the maximum of 13% at 30 min, and then decreased slowly to 9.5% at 300 min (see Fig. 6(c)). As a comparison, the YS, UTS and elongation of 520 °C-solutionized T6 bars were 257 MPa, 329 MPa and 11%, respectively, which have no distinct improvement over the 490 °C-solutionized ones.

During the age process, the main microstructure transformation was the precipitation reaction [12,15,22], which turned the $\alpha$-Al grains from homogeneous solid solution to the phase reinforced with precipitates inside. Those brittle precipitates could hinder the movement of dislocations during plastic deformation. Thus, the aging process improved the strength but lower the elongation compared with that of the as-quenched samples. However, the elongation of T6 state is still higher than that of as-cast state (see dash line in Fig. 6(c)).

### 3.3 Fractography

Figure 7 shows the fracture surface observed using SEM after the tensile test. Without solution treatment, the fracture surface exhibited more brittle features. The modified fiber-like eutectic Si, embedded deeply in the $\alpha$-Al matrix, and cracked during the tensile test (see Fig. 7(a)). The fracture mode changed as the solution treatment time increased. After 5-min solution treatment, some shallow dimples started to emerge on the fracture surface (see Fig. 7(b)). After solution treatment of 30 min, the fracture surface exhibited a uniform distribution of small dimples of ~2.5 μm (see Fig. 7(c)). Prolonged solution treatment, i.e., 300 min, only enlarged the dimple size to ~5 μm (see Fig. 7(d)). Some spherical Si particles sat at the bottoms of the dimples, as marked by the arrows in Fig. 7(d).

### 3.4 In-situ observation of deformation and crack

Figure 8 shows a typical microstructure during

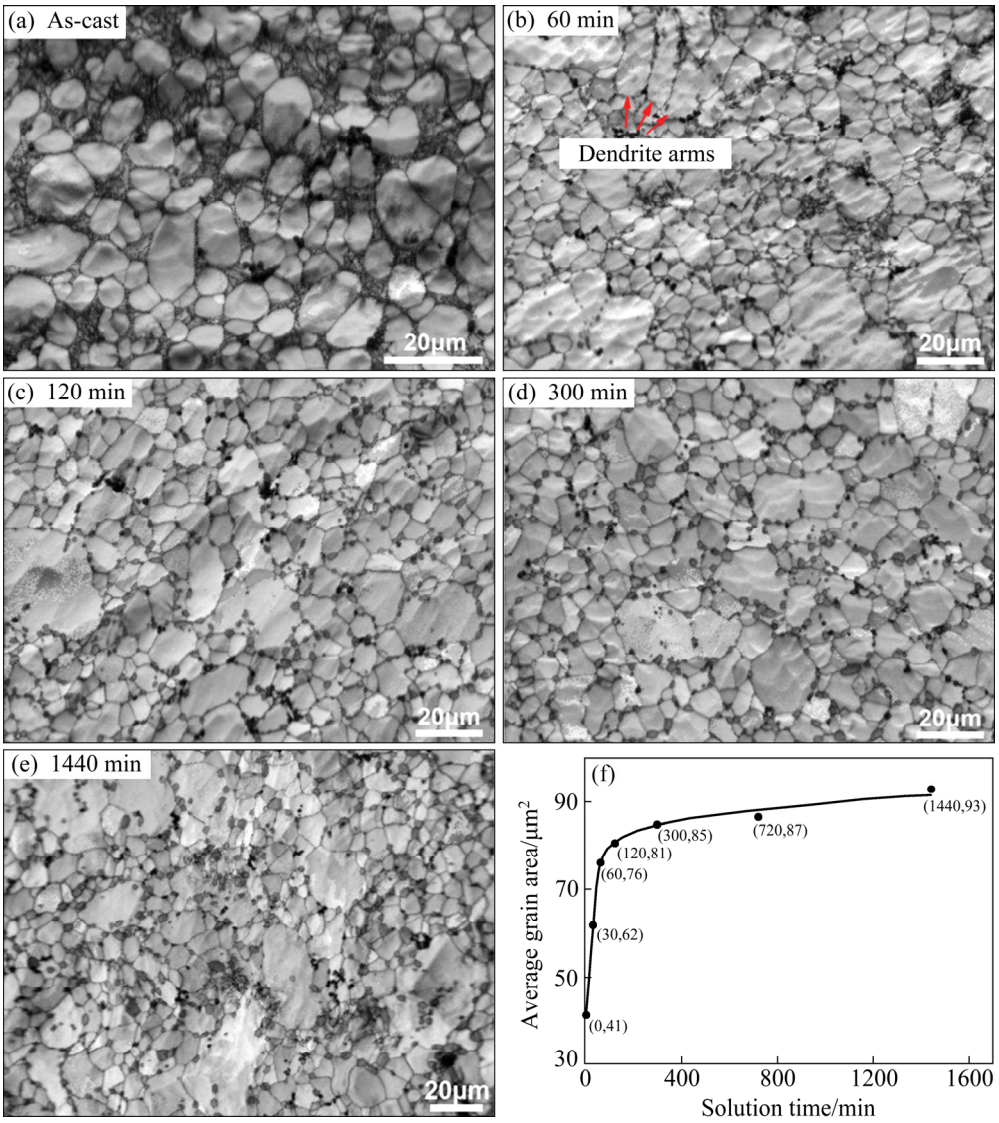


**Fig. 5** EBSD image quality maps of as-cast specimen (a) and specimens solutionized at 490 °C (b−e), and evolution of average grain area of $\alpha$-Al matrix versus solution time at 490 °C (f)

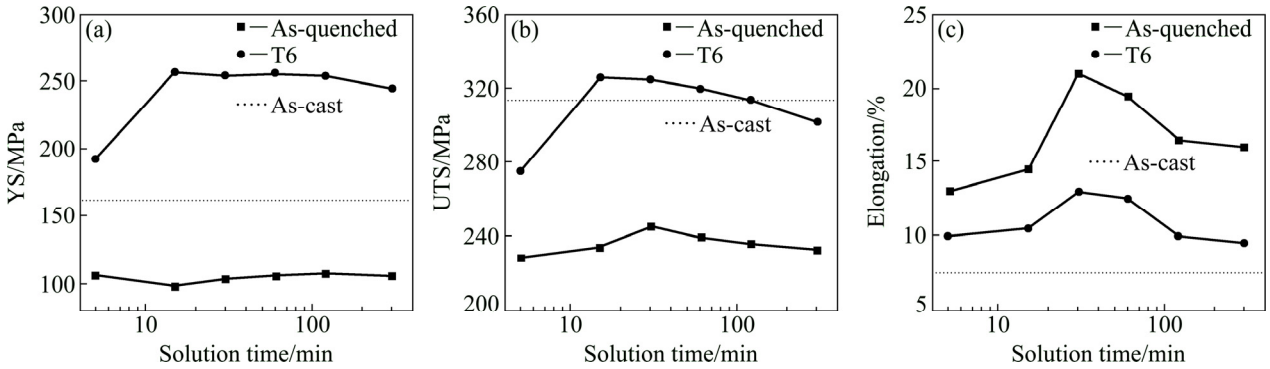


**Fig. 6** Mechanical properties of as-cast, as-quenched and T6 samples after solution treatment at 490 °C: (a) Yield strength (YS); (b) Ultimate tensile strength (UTS); (c) Elongation

in-situ tensile deformation. All the view fields were at the crack tip, where severe plastic deformation occurred. In the die-cast sample (see Figs. 8(a) and (b)), the $\alpha$-Al grains exhibited clear and uniform slip bands, indicating a uniform plastic deformation. The slip bands stopped in the eutectic region at the $\alpha$-Al grain boundary. The eutectic silicon was too stiff to deform continuously and harmoniously with the $\alpha$-Al grains, thus micro-cracks

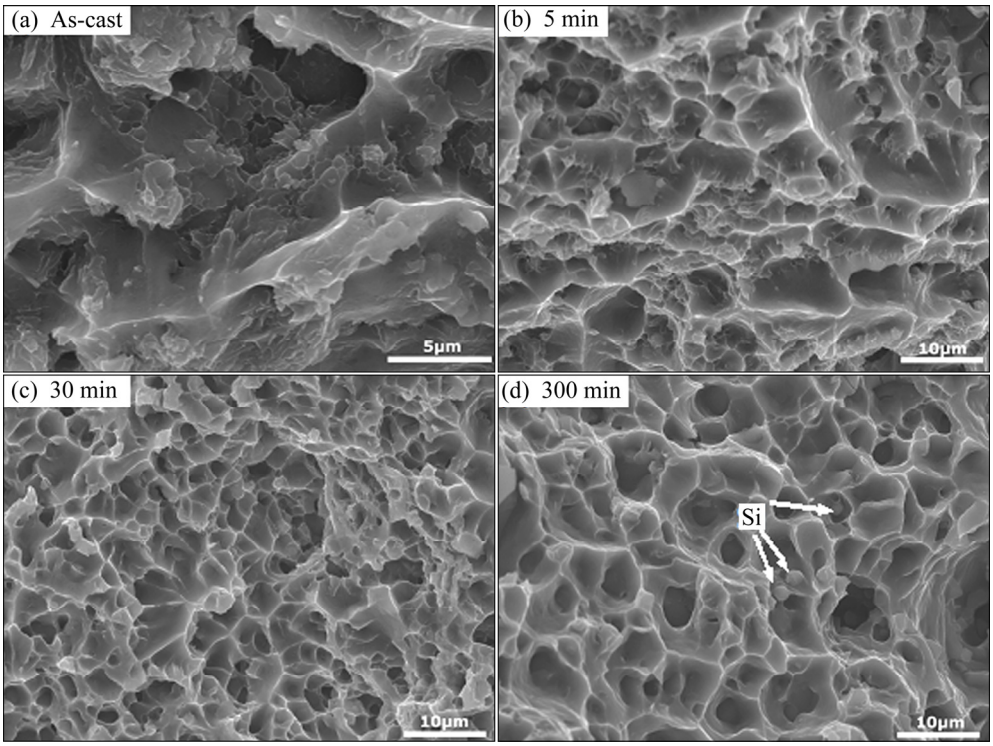


**Fig. 7** Fracture surfaces of as-cast sample (a) and T6-treated samples at different solution time (b−d)

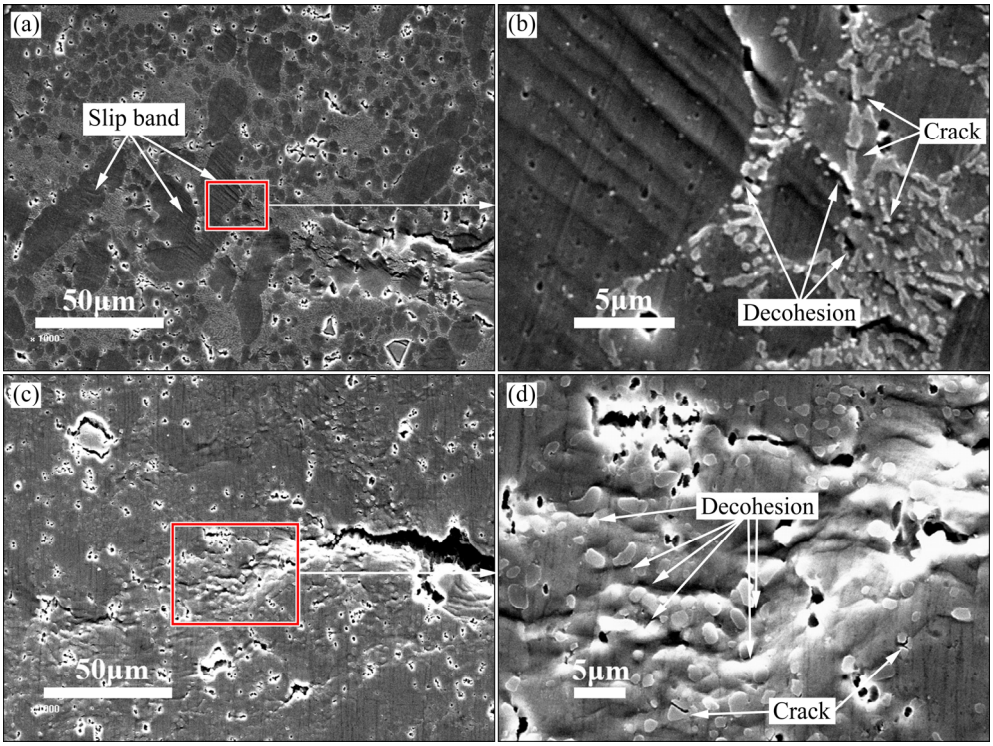


**Fig. 8** Deformation at main crack during in-situ tensile test for as-cast (a, b) and T6-treated (c, d) samples ((b) is magnified view of red square in (a), and (d) is magnified view of red square in (c))

generated. Both interface decohesion and brittle cracks could be observed (see Fig. 8(b)), i.e., as deformation proceeded, the crack expanded rapidly along the grain boundaries, as shown in Fig. 9(a).

In the T6-state sample (see Figs. 8(c) and (d)), the polished surface of specimen was significantly disturbed at the crack tip. The $\alpha$-Al grains still remained the capability of slipping after precipitation reaction because the low content of Mg limited the amount of strengthening precipitates. The slip bands were

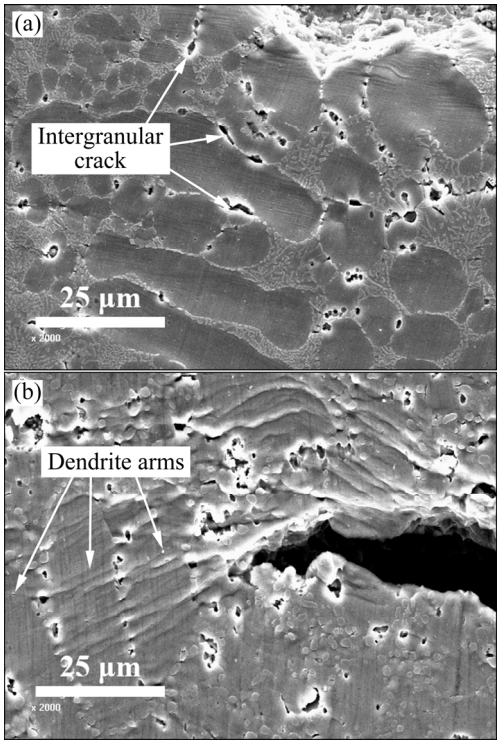


**Fig. 9** Grain boundaries after deformation for as-cast (a) and T6-treated (b) samples

disordered, coarse and prone to bifurcate. In Fig. 8(d), the Si particles scattered in the $\alpha$-Al matrix, indicating the presence of the eutectic before solution treatment. The intricate fiber-like Si network collapsed, and the slip bands could propagate deeply into the eutectic region. Without large aspect ratios and coarse interfaces, most Si particles detached from the $\alpha$-Al matrix at the interface due to deformation mismatch (see Fig. 8(d)). The plastic deformation smoothly transmitted from grain to grain, or from one dendrite arm to another without inter-granular cracking (see Fig. 9(b)). Meanwhile, small cracks generated at the interface, and became larger when external load was amplified. These minor cracks could act as the potential precursors of the main crack, thus the main crack expanded in zigzags and branched occasionally.

## 4 Discussion

### 4.1 Optimization of solution treatment temperature

Conventional practice suggests that ~540 °C is a recommended solution temperature for Al−Si−Mg alloy [4,5,23], in order to shorten the solution time. However, the risk of gas pore expansion and blistering was not taken into consideration because there are no high pressure gas pores inside the traditional castings. As shown in Fig. 2(f), blistering happened on the surface of die-cast tensile test bar only after solution treatment at 540 °C for 30 min.

The main concern of solution treatment of die castings is to finish solutionizing before serious pore expansion and blistering. One logical adjustment is lowering the solution temperature, at which the gas pressure in pores remains relatively low and the alloy still has competent strength to delay the pore expansion and blistering. In this study, most solution treatments were carried out at 490 °C, which was ~75 °C lower than the solidus line and ~67 °C lower than the eutectic reaction temperature (see Fig. 10). The experimental result indicated that distinct pore expansion happened very late at 490 °C (Figs. 2(b) and (c)). Besides, 490 °C was estimated to be just slightly higher than the solvus line to ensure the complete dissolution of $\beta$-$Mg_2Si$ phases, according to Fig. 10 [24,25]. Solution treatment experiment demonstrated that it took a short time to finish the dissolution of $\beta$-$Mg_2Si$ phases and the spheroidization of the eutectic silicon (see Fig. 4). Substantial improvement on mechanical properties could be achieved after aging process (see Fig. 6). The tensile test also demonstrated that the mechanical properties of 520 °C-solutionized T6-state bars have no distinct improvement over those of the 490 °C-solutionized ones.

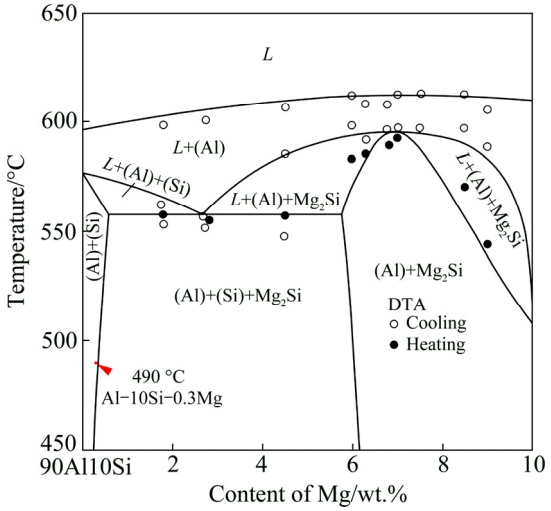


**Fig. 10** Computed vertical sections of phase diagram of Al−Mg−Si alloy with 90 wt.% Al [24,25]

The experiment mentioned above demonstrated that the solution treatment of die castings could be finished at a low temperature in a short time. That was the result of the fine microstructure of die castings (see Fig. 3). According to Fick's law, the evaluated diffusion distances, i.e., $\sqrt{Dt}$, were about 11.3 and 9.4 μm respectively, for Mg and Si, where $D$ was the diffusion coefficient in $\alpha$-Al matrix at solution temperature of 763 K [26], and $t$=900 s was the solution time. These distances exceeded the average dendrite arm radius, i.e.,

about 8 μm (see Figs. 4(a) and 5(a)), indicating that it was close to the completion of homogenization across the dendrite arms when the solution time was 15 min.

### 4.2 Silicon evolution during solution treatment

Altering the morphology of the eutectic silicon is one of the most important aims of solution treatment. Modified with Sr, the flaky Si turned into fiber-like morphology, which had been extensively studied [27,28]. The observation of deeply etched sample showed that the eutectic Si fibers were connected (see Fig. 3). However, the microstructure was unstable due to the vast and complicated interface between $\alpha$-Al grains and Si fibers. The modified Si was easier to fragment, as shown in Ref. [29].

The microstructure evolution is driven by the minimization of the total free energy of the system. This was achieved by reducing the interface area between Si phase and $\alpha$-Al matrix [30]. As a result of the Rayleigh−Taylor surface instability, unstable perturbations increased in amplitude before the connected area finally pinched off, and the fibrous silicon fragmented into discrete droplets [31,32]. The second stage was spheroidization, during which the droplets tended to decrease the interfacial curvature. Capillarity-induced diffusion gave rise to the apparent flux of solute from the region with high curvature to that with low curvature [33] as a result of Gibbs−Thomson effect. In that way, the specific interface area was reduced. Further reduction in interfacial energy of the system was accomplished with larger particles growing and smaller particles shrinking, i.e., the Ostwald ripening [34]. The growth of the silicon particles followed the traditional LSW (Lifshitz−Slyozow−Wagner) theory [35]:

$$\overline{R}^3 - \overline{R}_0^{\,3} = kt \quad (1)$$

where $t$ is the time, $\overline{R}$ is the average radius of the particles, $\overline{R}_0$ is the initial average radius at $t$=0, and $k$ is a constant. The evolution of the average radius of the particles fitted very well with Eq. (1) after 30-min solution treatment (see Fig. 11, the square of correlation coefficient of this linear regression is 0.993). The evolution of the silicon particles was a combination of fragmentation, spheroidization and Oswald ripening. As the Oswald ripening proceeded, the distribution of the particle radius was adjusted asymptotically following the LSW theory.

### 4.3 Effect of microstructure evolution on deformation and cracking

The morphology of the eutectic Si particles had a great influence on the mechanical properties of the alloy. As a brittle phase, the Si could either strengthen the matrix or promote crack nucleation.

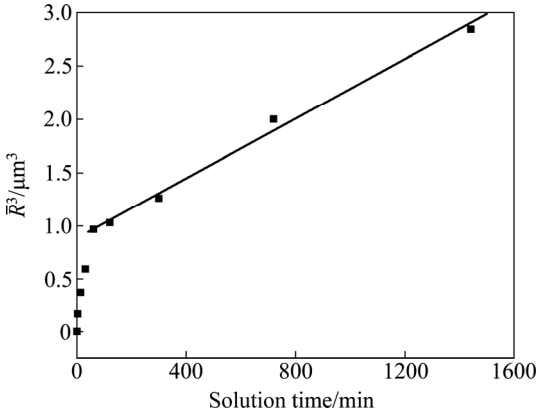


**Fig. 11** Cube of equivalent eutectic Si radius vs solution time

For die-cast specimen, the eutectic was divorced (see Fig. 3) as a consequence of extremely high cooling rate [1]. The configuration signified that the silicon−fiber-reinforced Al-matrix composite filled the inter-dendritic arm space and the inter-granular space of the $\alpha$-Al grains. The hard, brittle and semi-continuous (see Fig. 3(b)) silicon fibers comprised the skeleton to sustain the whole material and provided a great strengthening effect. The complicated interface between $\alpha$-Al grains and Si fibers ensured the sturdy cohesion. When external force exerted on the specimen, the fiber-like Si could bear a lot of load due to its higher elastic modulus and inflexibility for yield. So, the die-cast specimen exhibited a relatively high strength. On the other hand, the Si particles isolated the plastic $\alpha$-Al grains from each other (see Fig. 3(a)), and the plastic deformation in one $\alpha$-Al grain could not be compatible with that in its neighbors (see Figs. 8(a) and (b)), i.e., the potential ductility was significantly suppressed. As the external force increased, the plastic incompatibility between silicon fibers and $\alpha$-Al grains would ultimately lead to either silicon cracking or interface decohesion (see Fig. 8(b)), leading to an elongation of only ~7.5% (see Fig. 6(c)).

The skeleton began to decompose after 5-min solution treatment at 490 °C via necking and fragmentation of the fiber-like Si (Fig. 4(a)). The contribution of solute Mg atoms to yield strength is estimated to be less than 13 MPa, with the equation in Ref. [36]. The strengthening effect of the Si particles with small aspect ratio and smooth surface was much lower than that of the fibrous Si. Accordingly, both YS and UTS would decrease whereas the elongation increased (see Fig. 6). The fracture mode also changed during the 5-min solution treatment (see Fig. 7(b)). However, 5-min solution treatment was not enough to dissolve all the $\beta$-$Mg_2Si$ phases (see Fig. 4(a)), so the following artificial age could not make full use of Mg atoms in this alloy to strengthen the $\alpha$-Al matrix.

After fragmentation and spheroidization during 30-min solution treatment (see Fig. 4(c) and Fig. 7(c)), the $\alpha$-Al grains joined together to form a continuous matrix. Discontinuous Si droplets could not hinder all the moving dislocations across the borders, and neighboring $\alpha$-Al grains cooperated with each other efficiently during plastic deformation (see Figs. 8(c) and (d)). After the dissolution of $\beta$-$Mg_2Si$ phase, both Mg and Si atoms precipitated as meta-stable phases in the $\alpha$-Al grains during artificial age [12,15,22]. The corresponding T6-state strength reached the maximum value. Prolonged solution time could not provide higher supersaturation after water quenching. Thus, the strengthening effect of precipitation kept constant. However, the $\alpha$-Al grains coarsened (see Fig. 5(f)), which weakened the alloy strength according to Hall−Patch equation. Thus, the combined effect led to the decrease in mechanical properties (see Fig. 6).

When plastic deformation occurred, the dislocations in $\alpha$-Al grains moved forward to the grain boundaries, and stopped when encountering the Si particles. Further deformation and dislocation accumulation caused stress concentrations at the interface between $\alpha$-Al grains and Si particles [21,37]. When stress concentrations exceeded some critical values, crack would initiate either in the silicon particles or at the interface (see Fig. 8(d)). The actual crack mode was a very local event as a result of many factors [37]. According to the in-situ observation (see Fig. 8(d)), the latter cracking mode became dominant for the heat-treated specimen. The Si particles bound loosely with the $\alpha$-Al matrix. And because the micro-cracks could grow and expand along the interfaces, the Si particles were removed from the $\alpha$-Al matrix. Further deformation would lead to the join of the micro-cracks as well as the nucleation of new micro-cracks until the final fracture, leaving Si particles at the bottom of the dimple (see Fig. 7(d)).

After spheroidization, shorter solution treatment would be more beneficial to the ductility of the material due to smaller particles, shorter inter-particle spacing and larger population of particles. Firstly, despite their lack of the capacity for plastic deformation, those small spherical particles were more flexible to minimize the plastic incompatibility with matrix through movement and rotation (see Fig. 8(d)). Thus, the nominal stress required for particle cracking increased as particle size decreased [37]. Secondly, shorter inter-particle spacing implied shorter mean free path, less dislocation accumulation [38] at interface and lower stress concentration before the initial cracking. Regardless of the cracking mode, the size of the micro-crack reflected the magnitude of deformation incompatibility between the particles and the matrix. The stress concentration factor was proportional to the square root of the crack size, thus smaller inter-particle spacing would lead to smaller micro-cracks and lower stress concentration. Thirdly, severe plastic deformation would occur in front of the tip of cracks. Keeping constant volume fraction of particles during coarsening process, larger population of particles would lead to more micro-cracks. The deformed regions in front of micro-cracks would absorb more energy by work hardening. In this respect, large population of micro-cracks dispersed the plastic deformation, preventing severe strain localization and delaying the expansion of large cracks.

## 5 Conclusions

(1) Contrary to the conventional practice, the solution treatment of the die-cast AlSi10MnMg alloy should be carried out under a relatively low temperature in a shorter time. Substantial strengthening effect could be achieved in the following artificial aging process. Prolonging solution time and elevating solution temperature would be meaningless or even harmful due to microstructure coarsening, surface blistering and/or gravitational deflection.

(2) The Si particles changed rapidly during solution treatment. After the fragment and spheroidization, the coarsening process of Si particles followed the LSW equation.

(3) The morphology and the size of Si particles affected the mechanical properties and the fracture mode through affecting the interaction of $\alpha$-Al grains.

## References

[1] GUO Zhi-peng, XIONG Shou-mei, CHO S H, CHOI J K. Study on heat transfer behavior at metal/die interface in aluminum alloy die casting process. I: Experimental study and determination of the interfacial heat transfer coefficient [J]. Acta Metallurgica Sinica, 2007, 43: 1149−1154. (in Chinese)

[2] JIA Liang-rong, XIONG Shou-mei, LIU Bai-cheng. Study on numerical simulation of mold filling and heat transfer in die casting process [J]. Journal of Materials Science & Technology, 2000, 16: 269−272.

[3] OZHOGA-MASLOVSKAJA O, GARIBOLDI E, LEMKE J N. Conditions for blister formation during thermal cycles of Al−Si−Cu−Fe alloys for high pressure die-casting [J]. Materials & Design, 2016, 92: 151−159.

[4] YANG Chang-lin, LI Yuan-bing, DANG Bo, LÜ He-bin, LIU Feng. Effects of cooling rate on solution heat treatment of as-cast A356 alloy [J]. Transactions of Nonferrous Metals Society of China, 2015, 25: 3189−3196.

[5] DANG Bo, LIU Cong-cong, LIU Feng, LIU Ying-zhuo, LI Yuan-bing. Effect of as-solidified microstructure on subsequent solution-treatment process for A356 Al alloy [J]. Transactions of Nonferrous Metals Society of China, 2016, 26: 634−642.

[6] CAO Han-xue, HAO Meng-yao, SHEN Chao, LIANG Peng. The influence of different vacuum degree on the porosity and mechanical properties of aluminum die casting [J]. Vacuum, 2017, 146: 278−281.

[7] LI Xiao-bo, XIONG Shou-mei, GUO Zhi-peng. Improved

mechanical properties in vacuum-assist high-pressure die casting of AZ91D alloy [J]. Journal of Materials Processing Technology, 2016, 231: 1−7.

[8] LUMLEY R N, ODONNELL R G, GUNASEGARAM D R, GIVORD M. Heat treatment of high-pressure die castings [J]. Metallurgical and Materials Transactions A, 2007, 38: 2564−2574.

[9] LUMLEY R N, POLMEAR I J, CURTIS P R. Rapid heat treatment of aluminum high-pressure die castings [J]. Metallurgical and Materials Transactions A, 2009, 40: 1716−1726.

[10] YUAN Zi-hao, GUO Zhi-peng, XIONG Shou-mei. Effect of as-cast microstructure heterogeneity on aging behavior of a high-pressure die-cast A380 alloy [J]. Materials Characterization, 2018, 135: 278−286.

[11] YUAN Zi-hao, GUO Zhi-peng, XIONG Shou-mei. Different aging behaviors at surface layer and central region of a die-casting A380 alloy during heat treatment [J]. China Foundry, 2017, 14: 506−512.

[12] VLACH M, ČÍŽEK J, SMOLA B, MELIKHOVA O, VLČEK M, KODETOVÁ V, KUDRNOVÁ H, HRUŠKA P. Heat treatment and age hardening of Al−Si−Mg−Mn commercial alloy with addition of Sc and Zr [J]. Materials Characterization, 2017, 129: 1−8.

[13] GAO Guan-jun, HE Chen, LI Yong, LI Jia-dong, WANG Zhao-dong, MISRA R D K. Influence of different solution methods on microstructure, precipitation behavior and mechanical properties of Al−Mg−Si alloy [J]. Transactions of Nonferrous Metals Society of China, 2018, 28: 839−847.

[14] CUI Li-xin, LIU Zhen-xing, ZHAO Xiao-guang, TANG Jian-guo, LIU Ke, LIU Xing-xing, QIAN Chen. Precipitation of metastable phases and its effect on electrical resistivity of Al−0.96$Mg_2Si$ alloy during aging [J]. Transactions of Nonferrous Metals Society of China, 2014, 24: 2266−2274.

[15] DING Li-peng, JIA Zhi-hong, ZHANG Zhi-qing, SANDERS R E, LIU Qing, YANG Guang. The natural aging and precipitation hardening behaviour of Al−Mg−Si−Cu alloys with different Mg/Si ratios and Cu additions [J]. Materials Science and Engineering A, 2015, 627: 119−126.

[16] DWIVEDI D K, SHARMA R, KUMAR A. Influence of silicon content and heat treatment parameters on mechanical properties of cast Al−Si−Mg alloys [J]. International Journal of Cast Metals Research, 2006, 19: 275−282.

[17] LADOS D A, APELIAN D, WANG Li-bo. Solution treatment effects on microstructure and mechanical properties of Al−(1 to 13 pct) Si−Mg cast alloys [J]. Metallurgical and Materials Transactions B, 2011, 42: 171−180.

[18] LIN Yong-cheng, LUO Shun-cun, HUANG Jian, YIN Liang-xing, JIANG Xing-you. Effects of solution treatment on microstructures and micro-hardness of a Sr-modified Al−Si−Mg alloy [J]. Materials Science and Engineering A, 2018, 725: 530−540.

[19] FACCOLI M, DIONI D, CECCHEL S, CORNACCHIA G, PANVINI A. Optimization of heat treatment of gravity cast Sr-modified B356 aluminum alloy [J]. Transactions of Nonferrous Metals Society of China, 2017, 27: 1698−1706.

[20] ROMETSCH P, ARNBERG L, ZHANG D L. Modelling dissolution of $Mg_2Si$ and homogenisation in Al−Si−Mg casting alloys [J]. International Journal of Cast Metals Research, 1999, 12: 1−8.

[21] MISHNAEVSKY L L Jr, LIPPMANN N, SCHMAUDER S, GUMBSCH P. In-situ observation of damage evolution and fracture in AlSi7Mg0.3 cast alloys [J]. Engineering Fracture Mechanics, 1999, 63: 395−411.

[22] MILKEREIŤ B, STARINK M J. Quench sensitivity of Al−Mg−Si alloys: A model for linear cooling and strengthening [J]. Materials & Design, 2015, 76: 117−129.

[23] CHOI S W, KIM Y M, LEE K M, CHO H S, HONG S K, KIM Y C, KANG C S, KUMAI S. The effects of cooling rate and heat treatment on mechanical and thermal characteristics of Al−Si−Cu−Mg foundry alloys [J]. Journal of Alloys and Compounds, 2014, 617: 654−659.

[24] RAGHAVAN V. Al−Mg−Si (aluminum−magnesium−silicon) [J]. Journal of Phase Equilibria and Diffusion, 2007, 28: 174−179.

[25] FEUFEL H, GÖDECKE T, LUKAS H L, SOMMER F. Investigation of the Al−Mg−Si system by experiments and thermodynamic calculations [J]. Journal of Alloys and Compounds, 1997, 247: 31−42.

[26] XIN Jing-hua, ZHANG Wei-bin, WANG Jian-chuan, ZHAO Dong-dong, DU Yong, ZHANG Li-jun, HUANG Bai-yun. Prediction of diffusivities in fcc phase of the Al−Cu−Mg system: First-principles calculations coupled with CALPHAD technique [J]. Computational Materials Science, 2014, 90: 32−43.

[27] MAZAHERY A, SHABANI M O. Modification mechanism and microstructural characteristics of eutectic Si in casting Al−Si alloys: A review on experimental and numerical studies [J]. JOM, 2014, 66: 726−738.

[28] ZHANG Yong, ZHENG Hong-liang, LIU Yue, SHI Lei, XU Rong-fu, TIAN Xue-lei. Cluster-assisted nucleation of silicon phase in hypoeutectic Al−Si alloy with further inoculation [J]. Acta Materialia, 2014, 70: 162−173.

[29] ZHANG D L, ZHENG L H, STJOHN D H. Effect of a short solution treatment time on microstructure and mechanical properties of modified Al−7wt.%Si−0.3wt.%Mg alloy [J]. Journal of Light Metals, 2002, 2: 27−36.

[30] RATKE L, VOORHEES P W. Growth and coarsening [M]. Heidelberg: Springer, 2002.

[31] AAGESEN L K, JOHNSON A E, FIFE J L, VOORHEES P W, MIKSIS M J, POULSEN S O, LAURIDSEN E M, MARONE F, STAMPANONI M. Pinch-off of rods by bulk diffusion [J]. Acta Materialia, 2011, 59: 4922−4932.

[32] AAGESEN L K, JOHNSON A E, FIFE J L, VOORHEES P W, MIKSIS M J, POULSEN S O, LAURIDSEN E M, MARONE F, STAMPANONI M. Universality and self-similarity in pinch-off of rods by bulk diffusion [J]. Nature Physics, 2010, 6: 796−800.

[33] AARON H B, KOTLER G R. Second phase dissolution [J]. Metallurgical Transactions, 1971, 2: 393−408.

[34] VOORHEES P W, GLICKSMAN M E. Solution to the multi-particle diffusion problem with applications to Ostwald ripening. I: Theory [J]. Acta Metallurgica, 1984, 32: 2001−2011.

[35] LIFSHITZ I M, SLYOZOV V V. The kinetics of precipitation from supersaturated solid solutions [J]. Journal of Physics and Chemistry of Solids, 1961, 19: 35−50.

[36] SIMAR A, BRÉCHET Y, de MEESTER B, DENQUIN A, GALLAIS C, PARDOEN T. Integrated modeling of friction stir welding of 6xxx series Al alloys: Process, microstructure and properties [J]. Progress in Materials Science, 2012, 57: 95−183.

[37] YEH Jien-wei, LIU Wen-pin. The cracking mechanism of silicon particles in an A357 aluminum alloy [J]. Metallurgical and Materials Transactions A, 1996, 27: 3558−3568.

[38] ANTOLOVICH S D, ARMSTRONG R W. Plastic strain localization in metals: Origins and consequences [J]. Progress in Materials Science, 2014, 59: 1−160.

# 固溶处理过程中变质 AlSi10MnMg 压铸铝合金的组织演化及其对力学性能的影响

袁梓豪[1]，郭志鹏[1]，熊守美[1,2]

1. 清华大学 材料学院，北京 100084；
2. 清华大学 汽车安全与节能国家重点实验室，北京 100084

**摘　要**：为了优化变质 AlSi10MnMg 压铸合金的固溶工艺，采用 OM、SEM、EBSD 和拉伸试验研究固溶处理对合金组织、力学性能和断裂机制的影响。结果显示，固溶处理可在比传统工艺更低温度、更短时间的条件下完成，能避免表面鼓泡，并在随后的时效过程中获得较好的强化效果。延长固溶时间、提高固溶温度不能提高时效后合金的强度，甚至会对其产生不利影响。固溶过程中(尤其是早期)共晶硅形态的快速演化影响 $\alpha$-Al 晶粒间的相互作用，进而改变最终的力学性能和断裂模式。

**关键词**：AlSi10MnMg 合金；压铸；固溶处理；组织演化；力学性能；工艺优化

**(Edited by Wei-ping CHEN)**